Pergamon

Int. J. Solids Structures Vol. 31, No. 3, pp. 329–345, 1994

0020–7683/94 $6.00 + .00

INTERFACE CRACK LOADED BY A TIME-HARMONIC PLANE WAVE

JIANMIN QU
George W. Woodruff School of Mechanical Engineering, Georgia Institute of Technology, Atlanta, GA 30332-0405, U.S.A.

(*Received* 26 *March* 1993; *in revised form* 30 *July* 1993)

Abstract—In this paper, the two-dimensional problem of a finite crack along the interface between two dissimilar solids loaded by a plane wave is considered. Through use of the Fourier transform method, the boundary value problem of wave scattering is reduced to a vectorial Cauchy singular integral equation for the dislocation density on the crack face. A Jacobi polynomial technique is then used to solve the integral equation numerically. Crack opening displacements and stress intensity factors are obtained for various incident frequencies and incident angles. It is found that the crack faces interpenetrate each other near the crack-tips, and the crack-tip singular fields are oscillatory. The oscillatory index is the same as that for an interface crack under static loading, which can be expressed by the second Dundurs bimaterial constant. For practical purposes, an engineering approximation is proposed to remedy these pathological behaviors near the crack tips.

1. INTRODUCTION

Cracks are likely to occur on grain boundaries and bimaterial interfaces in polycrystal alloys and composite materials. It is, therefore, of practical importance to be able to assess the stress fields near such interface cracks, and to be able to detect them by non-destructive means. The goal of this paper is to contribute to the theoretical basis for the study of interface cracks under dynamic loading, and for the detection of interfacial flaws by ultrasonic techniques.

Specifically, the two-dimensional problem of a finite crack along the interface between two dissimilar solids loaded by a plane wave is considered. The dissimilar solids are taken to be isotropic, and linearly elastic. The incident plane wave is assumed to be time harmonic. Through the Fourier transform method, the boundary value problem of wave scattering is reduced to a vectorial Cauchy singular integral equation for the dislocation density on the crack face. A Jacobi polynomial technique is then used to solve the integral equation numerically. Crack opening displacements and stress intensity factors are obtained for various incident frequencies and incident angles. It is found that the crack faces interpenetrate each other near the crack tips, and the crack-tip singular fields are oscillatory, as observed by Yang and Bogy (1985). The oscillatory index is the same as that for an interface crack under static loading, which can be expressed by the second Dundurs bimaterial constant. For practical purposes, an engineering approximation is proposed to remedy these pathological behaviors near the crack tips.

Interaction of elastic waves with cracks in homogeneous media has been studied extensively in the past two decades. For example, Mal (1970a,b) studied both two-dimensional Griffith cracks and three-dimensional penny-shaped cracks by the Fourier transform method. High frequency approximation of the stress intensity factors is presented by Achenbach and Gautesen (1978). However, there seems to be very little study on the interaction of elastic waves with interface cracks. Several previously published works that bear directly on this problem are cited here. Boström (1987) solved the problem of scattering by a finite interface crack for antiplane strain deformation. When the second Dundurs bimaterial constant is zero, the crack-tip fields become non-oscillatory. In this case, Yang and Bogy (1985) solved for the stress intensity factors of an interface crack in a layered half space under normal incidence. Assuming the dissimilar solids are joined together by linear springs, Hirose and Kitahara studied the problem by the boundary element method.

The corresponding interface crack problem under static loading has been studied extensively since the early 1960s [e.g., Williams (1959), Erdogan (1965), Rice and Sih (1965)

and England (1965), among others]. Recently, the problem of a finite crack along the interface between two anisotropic dissimilar solids under static loading has been studied by several investigators (Willis, 1971; Qu and Bassani, 1989; Qu and Li, 1991; Suo, 1991).

2. PROBLEM STATEMENT

Consider a crack of length $2a$ on the interface between two dissimilar, linearly elastic solids, as shown in Fig. 1. λ_j, μ_j and ρ_j are used to denote the Lamé constants and the mass density of material $j (j = 1, 2)$, respectively. A Cartesian coordinate system (x_1, x_2) is assumed such that the x_1-axis is along the interface, and the x_2-axis is pointing to material 2.

Let the incident wave be a plane, time harmonic wave from $x_2 = -\infty$. With the time factor $\exp(-i\omega t)$ omitted throughout this paper, the incident wave may be written as

$$\mathbf{u}^{(i)}(x_1, x_2) = u_0 \mathbf{d}^{(\alpha)} \exp[ik_\alpha^{(1)}(x_1 p_1 + x_2 p_2)], \quad \alpha = L, T, \tag{1}$$

where

$$\begin{bmatrix} p_1 \\ p_2 \end{bmatrix} = \begin{bmatrix} \sin\theta_i \\ \cos\theta_i \end{bmatrix} \tag{2}$$

is the propagating vector, and θ_i is the angle of incidence measured counter-clockwise from the negative x_2-axis. In (1), $k_\alpha^{(j)}$ is the longitudinal ($\alpha = L$), or transverse ($\alpha = T$) wave-number in material j. $\mathbf{d}^{(\alpha)}$ is the unit displacement vector related to the angle of incidence by

$$\mathbf{d}^{(L)} = \begin{bmatrix} \sin\theta_i \\ \cos\theta_i \end{bmatrix}, \quad \mathbf{d}^{(T)} = \begin{bmatrix} -\cos\theta_i \\ \sin\theta_i \end{bmatrix}. \tag{3}$$

By linear superposition, the total displacement field caused by the incident wave (1) can be written as

$$\mathbf{u}^{\text{total}} = \begin{cases} \mathbf{u}^{(i)} + \mathbf{u}^{(r)} + \mathbf{u}_1 & \text{when } x_2 < 0, \\ \mathbf{u}^{(t)} + \mathbf{u}_2 & \text{when } x_2 > 0, \end{cases} \tag{4}$$

where $\mathbf{u}^{(r)}$ and $\mathbf{u}^{(t)}$ are, respectively, the reflected and transmitted waves computed in the absence of the interface crack. $\mathbf{u}_1$ and $\mathbf{u}_2$ are the scattered fields in materials 1 and 2, respectively, in the presence of the interface crack. Since $\mathbf{u}^{(r)}$ and $\mathbf{u}^{(t)}$ are well known [e.g. Achenbach (1973)], the purpose of this paper is to solve for the scattered fields $\mathbf{u}_1$ and $\mathbf{u}_2$.

By using Hooke's law for linear elastic solids, the corresponding stress field can be written as

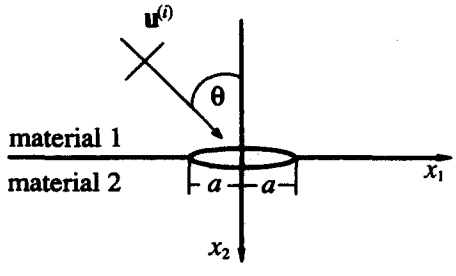

Fig. 1. An interface crack.

$$\boldsymbol{\sigma}^{\text{total}} = \begin{cases} \boldsymbol{\sigma}^{(i)} + \boldsymbol{\sigma}^{(r)} + \boldsymbol{\sigma}_1 & \text{when } x_2 < 0, \\ \boldsymbol{\sigma}^{(t)} + \boldsymbol{\sigma}_2 & \text{when } x_2 > 0. \end{cases} \tag{5}$$

For convenience, the traction vector on any plane parallel to the interface is defined by

$$\mathbf{t}(x_1, x_2) = \boldsymbol{\sigma}(x_1, x_2) \begin{bmatrix} 0 \\ 1 \end{bmatrix}. \tag{6}$$

It thus follows from (5) that

$$\mathbf{t}^{\text{total}} = \begin{cases} \mathbf{t}^{(i)} + \mathbf{t}^{(r)} + \mathbf{t}_1 & \text{when } x_2 < 0, \\ \mathbf{t}^{(t)} + \mathbf{t}_2 & \text{when } x_2 > 0. \end{cases} \tag{7}$$

It is assumed that the two solids are perfectly bonded together and the crack is fully open. This leads to the following boundary conditions for the total fields:

$$\mathbf{u}^{\text{total}}(x_1, -0) = \mathbf{u}^{\text{total}}(x_1, +0), \quad \text{for } |x_1| > a, \tag{8a}$$

$$\mathbf{t}^{\text{total}}(x_1, -0) = \mathbf{t}^{\text{total}}(x_1, +0), \quad \text{for any } x_1, \tag{8b}$$

$$\mathbf{t}^{\text{total}}(x_1, -0) = \mathbf{t}^{\text{total}}(x_1, +0) = \mathbf{0}, \quad \text{for } |x_1| < a. \tag{8c}$$

Note that for any x_1 the reflected and transmitted waves in the absence of the crack satisfy [see Achenbach (1973)]

$$\mathbf{u}^{(i)}(x_1, 0) + \mathbf{u}^{(r)}(x_1, 0) = \mathbf{u}^{(t)}(x_1, 0), \tag{9a}$$

$$\mathbf{t}^{(i)}(x_1, 0) + \mathbf{t}^{(r)}(x_1, 0) = \mathbf{t}^{(t)}(x_1, 0). \tag{9b}$$

Therefore, substituting (4) and (7) into (8) in conjunction with (9) yields

$$\mathbf{u}_1(x_1, 0) = \mathbf{u}_2(x_1, 0), \quad \text{for } |x_1| > a, \tag{10a}$$

$$\mathbf{t}_1(x_1, 0) = \mathbf{t}_2(x_1, 0), \quad \text{for any } x_1, \tag{10b}$$

$$\mathbf{t}_1(x_1, 0) = \mathbf{t}_2(x_1, 0) = -\mathbf{t}_0(x_1), \quad \text{for } |x_1| < a, \tag{10c}$$

where

$$\mathbf{t}_0 = \mathbf{t}^{(i)} + \mathbf{t}^{(r)}. \tag{11}$$

Expressions of $\mathbf{t}_0(x_1)$ are given in Appendix A.

Equations (10a–c) provide enough boundary conditions to uniquely determine $\mathbf{u}_1$ and $\mathbf{u}_2$ if the radiation conditions

$$\mathbf{u}_1(x_1, x_2) \to 0 \quad \text{as } |x_1| \to \infty, x_2 \to -\infty, \tag{12a}$$

$$\mathbf{u}_2(x_1, x_2) \to 0 \quad \text{as } |x_1| \to \infty, x_2 \to \infty, \tag{12b}$$

are also enforced.

3. THE INTEGRAL EQUATION

In this section, the Fourier transform method will be used to derive a system of Cauchy singular integral equations to solve for the scattered fields $\mathbf{u}_n(x_1, x_2)$. To this end, let

$$\mathbf{u}_n = \int_{-\infty}^{\infty} \mathbf{A}_n(\xi)\mathbf{E}_n(\xi, x_2)\mathbf{b}_n(\xi) \exp(-i\xi x_1 k_T^{(1)})\, d\xi, \tag{13}$$

where

$$\mathbf{A}_n(\xi) = \begin{bmatrix} -i\xi & (-1)^n i\gamma_T^{(n)} \\ (-1)^n i\gamma_L^{(n)} & i\xi \end{bmatrix}, \tag{14}$$

$$\mathbf{E}_n(\xi, x_2) = \begin{bmatrix} \exp[(-1)^n i\gamma_L^{(n)} k_T^{(1)} x_2] & 0 \\ 0 & \exp[(-1)^n i\gamma_T^{(n)} k_T^{(1)} x_2 \end{bmatrix}, \tag{15}$$

$$\gamma_\alpha^{(n)} = \begin{cases} \sqrt{(\hat{k}_\alpha^{(n)})^2 - \xi^2}, & \text{for } |\xi| < \hat{k}_\alpha^{(n)}, \\ i\sqrt{\xi^2 - (\hat{k}_\alpha^{(n)})^2}, & \text{for } |\xi| \geqslant \hat{k}_\alpha^{(n)}, \end{cases} \tag{16}$$

$$\hat{k}_\alpha^{(n)} = \frac{k_\alpha^{(n)}}{k_T^{(1)}} = \frac{c_T^{(1)}}{c_\alpha^{(n)}}, \quad \alpha = L, T, \quad n = 1, 2. \tag{17}$$

It can be shown by direct substitution that (13) satisfies the displacement equations of motion and the radiation conditions (12a–b) for any vector function $\mathbf{b}_n(\xi)$, which is to be determined by the boundary conditions (10a–c).

The corresponding traction vector can be obtained from (13) through Hooke's law for isotropic, linearly elastic materials

$$\mathbf{t}_n = \int_{-\infty}^{\infty} k_T^{(1)} \mathbf{B}_n(\xi)\mathbf{E}_n(\xi, x_2)\mathbf{b}_n(\xi) \exp(-i\xi x_1 k_T^{(1)})\, d\xi, \tag{18}$$

where

$$\mathbf{B}_n(\xi) = \mu_n \begin{bmatrix} 2(-1)^n \xi\gamma_L^{(n)} & 2\xi^2 - (\hat{k}_T^{(n)})^2 \\ 2\xi^2 - (\hat{k}_T^{(n)})^2 & -2(-1)^n \xi\gamma_T^{(n)} \end{bmatrix}. \tag{19}$$

To determine the unknown vector $\mathbf{b}_n(\xi)$, boundary conditions (10a–c) must be used. First, the traction continuity condition (10b) implies

$$\mathbf{B}_1\mathbf{b}_1 = \mathbf{B}_2\mathbf{b}_2 = \mathbf{h}. \tag{20}$$

Thus, on the crack face (10c) becomes

$$\int_{-\infty}^{\infty} k_T^{(1)} \mathbf{h}(\xi) \exp(-i\xi x_1 k_T^{(1)})\, d\xi = -\mathbf{t}_0(x_1). \tag{21}$$

Furthermore, define the crack opening displacement and the dislocation density, respectively, by

$$\Delta\mathbf{u}(x_1) = \mathbf{u}_2(x_1, 0) - \mathbf{u}_1(x_1, 0), \quad \mathbf{f}(x_1) = \frac{d}{dx_1}[\Delta\mathbf{u}(x_1)]. \tag{22a, b}$$

It then follows from (10a) that

$$-\mathrm{i}\int_{-\infty}^{\infty} k_{\mathrm{T}}^{(1)}\,\xi\{\mathbf{A}_2\mathbf{B}_2^{-1}-\mathbf{A}_1\mathbf{B}_1^{-1}\}\,\mathbf{h}\exp(-\mathrm{i}\xi x_1 k_{\mathrm{T}}^{(1)})\,\mathrm{d}\xi = \mathbf{f}(x_1)H(a^2-x_1^2), \tag{23}$$

where $H(x)$ is the Heaviside step function. Taking the inverse Fourier transform of (23) yields

$$\mathbf{h} = \frac{\mathrm{i}}{2\pi\xi}\mathbf{M}(\xi)\int_{-a}^{a}\mathbf{f}(\eta)\exp(\mathrm{i}\eta\xi k_{\mathrm{T}}^{(1)})\,\mathrm{d}\eta, \tag{24}$$

where

$$\mathbf{M}(\xi) = (\mathbf{A}_2\mathbf{B}_2^{-1}-\mathbf{A}_1\mathbf{B}_1^{-1})^{-1}. \tag{25}$$

Substitution of (24) into (21) results in an integral equation for the dislocation density

$$k_{\mathrm{T}}^{(1)}\int_{-a}^{a}\mathbf{K}_0(\eta-x_1)\mathbf{f}(\eta)\,\mathrm{d}\eta = -\mathbf{t}_0(x_1), \tag{26}$$

where the kernel is given formally by

$$\mathbf{K}_0(x) = \frac{\mathrm{i}}{2\pi}\int_{-\infty}^{\infty}\xi^{-1}\mathbf{M}(\xi)\exp(\mathrm{i}\xi x k_{\mathrm{T}}^{(1)})\,\mathrm{d}\xi. \tag{27}$$

In addition to the integral equation, the following compatibility equation is also required due to (22),

$$\int_{-a}^{a}\mathbf{f}(x_1)\,\mathrm{d}x_1 = \mathbf{0}. \tag{28}$$

Once the integral equation (26) is solved for the dislocation density $\mathbf{f}$, the vector $\mathbf{h}$ can be computed from (24). Consequently, $\mathbf{b}_n$ can be obtained from (20). Once $\mathbf{b}_n$ is known, the displacement and stress fields everywhere can be evaluated from (13) and (18), respectively, and the problem is solved.

In the following, (26) will be reduced to a standard Cauchy singular integral equation of the second kind. To this end, let us introduce

$$\alpha = \frac{\mu_2\kappa_1^2(\kappa_2^2-1)-\mu_1\kappa_2^2(\kappa_1^2-1)}{\mu_2\kappa_1^2(\kappa_2^2-1)+\mu_1\kappa_2^2(\kappa_1^2-1)}, \quad \beta = \frac{\mu_2(\kappa_2^2-1)-\mu_1(\kappa_1^2-1)}{\mu_2\kappa_1^2(\kappa_2^2-1)+\mu_1\kappa_2^2(\kappa_1^2-1)}, \tag{29a, b}$$

where

$$\kappa_n = \frac{k_{\mathrm{T}}^{(n)}}{k_{\mathrm{L}}^{(n)}} = \frac{c_{\mathrm{L}}^{(n)}}{c_{\mathrm{T}}^{(n)}} = \sqrt{\frac{2(1-\nu_n)}{1-2\nu_n}}, \tag{30}$$

in which ν_n is the Poisson ratio for material n. It can be easily shown that α and β defined by (29a, b) are the two Dundurs (1969) bimaterial constants for plane strain deformation.

Next, consider the $\mathbf{M}$ matrix given by (25). After some cumbersome asymptotic analysis, one can show that, as $\xi \to \pm\infty$

$$\xi^{-1}\mathbf{M}(\xi) = m[\mathrm{i}\beta\mathbf{I}_0-\mathrm{sgn}(\xi)\mathbf{I}]+O(\xi^{-2}), \tag{31}$$

where sgn (x) is the sign function, $\mathbf{I}$ is the identity matrix, and

$$m = \mu_1 \left(1 - \frac{1}{\kappa_1^2}\right)\left(\frac{1+\alpha}{1-\beta^2}\right), \tag{32}$$

$$\mathbf{I}_0 = \begin{bmatrix} 0 & 1 \\ -1 & 0 \end{bmatrix}. \tag{33}$$

Next, recall (Lighthill, 1964) that

$$\int_{-\infty}^{\infty} \exp(i\xi x)\, d\xi = 2\pi\delta(x), \tag{34a}$$

$$\int_{-\infty}^{\infty} \operatorname{sgn}(\xi) \exp(i\xi x)\, d\xi = \frac{2i}{x}, \tag{34}$$

where $\delta(x)$ is the Dirac delta function. Therefore, the kernel given by (27) can be rewritten as

$$\mathbf{K}_0(x) = -m\left\{\mathbf{K}(x) + \beta\delta(xk_T^{(1)})\mathbf{I}_0 - \frac{1}{\pi x k_T^{(1)}}\mathbf{I}\right\}, \tag{35}$$

in which

$$\mathbf{K}(x) = \frac{i}{2\pi}\int_{-\infty}^{\infty} \xi^{-1}\{i\xi\beta\mathbf{I}_0 - |\xi|\mathbf{I} - \mathbf{M}(\xi)/m\} \exp(i\xi x k_T^{(1)})\, d\xi. \tag{36}$$

Because of (31), it is obvious that $\mathbf{K}$ is well defined.

Substituting (35) into (26) yields the desired Cauchy singular integral equation of the second kind

$$\beta\mathbf{I}_0\mathbf{f}(x_1) - \frac{1}{\pi}\int_{-a}^{a} \frac{\mathbf{f}(\eta)}{\eta - x_1}\, d\eta + k_T^{(1)}\int_{-a}^{a} \mathbf{K}(\eta - x_1)\mathbf{f}(\eta)\, d\eta = \mathbf{t}_0(x_1)/m. \tag{37}$$

This integral equation cannot be solved analytically. Numerical solutions are presented in the next section.

To close this section, it is observed that

$$\mathbf{M} = (\mathbf{L} + \mathbf{S})^{-1}, \tag{38}$$

where

$$\mathbf{L} = \mathbf{L}_2 + \mathbf{L}_1, \quad \mathbf{S} = \mathbf{S}_2 - \mathbf{S}_1, \tag{39}$$

$$\mathbf{L}_n = \frac{-i(\hat{k}_T^{(n)})^2}{\mu_n\{4\xi^2\gamma_L^{(n)}\gamma_T^{(n)} + [2\xi^2 - (\hat{k}_T^{(n)})^2]^2\}}\begin{bmatrix} \gamma_T^{(n)} & 0 \\ 0 & \gamma_L^{(n)} \end{bmatrix}, \tag{40}$$

$$\mathbf{S}_n = \frac{i\xi[(\hat{k}_T^{(n)})^2 - 2\gamma_L^{(n)}\gamma_T^{(n)} - 2\xi^2]}{\mu_n\{4\xi^2\gamma_L^{(n)}\gamma_T^{(n)} + [2\xi^2 - (\hat{k}_T^{(n)})^2]^2\}}\mathbf{I}_0. \tag{41}$$

Obviously, when the two solids are identical, $\mathbf{S} = \mathbf{0}$ and $\alpha = \beta = 0$. In this case,

$$\mathbf{K}(x) = \frac{-\mathrm{i}}{2\pi}\int_{-\infty}^{\infty} \xi^{-1}\{\mathbf{L}^{-1}(\xi)/m + |\xi|\mathbf{I}\}\exp(\mathrm{i}\xi x k_{\mathrm{T}}^{(1)})\,\mathrm{d}\xi, \tag{42}$$

and the integral equation reduces to the first kind

$$\frac{-1}{\pi}\int_{-a}^{a}\frac{\mathbf{f}(\eta)}{\eta - x_1}\mathrm{d}\eta + k_{\mathrm{T}}^{(1)}\int_{-a}^{a}\mathbf{K}(\eta - x_1)\mathbf{f}(\eta)\,\mathrm{d}\eta = \mathbf{t}(x_1)/m. \tag{43}$$

This is the governing equation for a Griffith crack of length $2a$ in a homogeneous solid.

4. NUMERICAL SOLUTION OF THE INTEGRAL EQUATION

First, let us define

$$\mathbf{R} = \begin{bmatrix} -\mathrm{i} & 1 \\ 1 & -\mathrm{i} \end{bmatrix}, \quad D = \begin{bmatrix} \mathrm{i} & 0 \\ 0 & -\mathrm{i} \end{bmatrix}. \tag{44a, b}$$

Then, by introducing

$$\mathbf{f}(ax) = \mathbf{R}\mathbf{g}(x), \quad \mathbf{H}(x) = \mathbf{R}^{-1}\mathbf{I}_0^{-1}\mathbf{K}(ax)\mathbf{R}, \quad \mathbf{q}(x) = \mathbf{R}^{-1}\mathbf{I}_0^{-1}\mathbf{t}(ax)/m \tag{45a, b, c}$$

one can rewrite (37) as

$$\beta\mathbf{g}(x) + \frac{1}{\pi}\int_{-1}^{1}\mathbf{D}\mathbf{g}(\xi)\frac{\mathrm{d}s}{\xi - x}\xi + k_0\int_{-1}^{1}\mathbf{H}(\xi - x)\mathbf{g}(\xi)\,\mathrm{d}\xi = \mathbf{q}(x), \quad |x| < 1, \tag{46}$$

where $k_0 = ak_{\mathrm{T}}^{(1)}$ is the nondimensional wavenumber. Furthermore, since $\mathbf{R}$ is non-singular, the compatibility condition (28) becomes equivalent to

$$\int_{-1}^{1}\mathbf{g}(x)\,\mathrm{d}x = \mathbf{0}. \tag{47}$$

Equation (46) is a non-dimensional Cauchy singular integral equation of the second kind. A solution having integrable singularities at the end points, $x = \pm 1$, and satisfying the compatibility condition (47) will be obtained in this section. The solution procedure is based on the Jacobi polynomial expansion technique introduced by Erdogan (1969). A brief outline of this method is given below.

The fundamental solution which characterizes the singular behavior of $\mathbf{g}(x)$ at $x = \pm 1$ is given by Muskhelishvili (1953) as

$$\mathbf{W}(x) = \begin{bmatrix} (1-x)^{\eta_1}(1+x)^{\eta_2} & 0 \\ 0 & (1-x)^{\eta_2}(1+x)^{\eta_1} \end{bmatrix}, \tag{48a, b}$$

where

$$\eta_{1,2} = -\tfrac{1}{2} \mp \mathrm{i}\varepsilon, \quad \varepsilon = \frac{1}{2\pi}\ln\left(\frac{1+\beta}{1-\beta}\right). \tag{49}$$

The solution to (46) may be approximated by a Jacobi polynomial

$$\mathbf{g}(x) = \mathbf{W}(x) \sum_{n=1}^{N} \mathbf{P}_n(x)\mathbf{c}_n, \tag{50}$$

where $\mathbf{c}_n$ is a constant vector to be determined, and

$$\mathbf{P}_n(x) = \begin{bmatrix} P_n^{(\eta_1,\eta_2)} & 0 \\ 0 & P_n^{(\eta_2,\eta_1)}(x) \end{bmatrix}. \tag{51}$$

In (51), $P_n^{(\eta_1,\eta_2)}(x)$ is the nth order Jacobi polynomial (Abramowitz and Stegun, 1972).

Orthogonality of the Jacobi polynomials yields

$$\int_{-1}^{1} \mathbf{P}_m(x)\mathbf{W}(x)\mathbf{P}_n(x)\,\mathrm{d}x = d_m\delta_{mn}\mathbf{I} \quad \text{(no sum over } m\text{)}, \tag{52}$$

where, in terms of Gamma function $\Gamma(x)$,

$$d_m = \frac{2^{\eta_1+\eta_2+1}\Gamma(m+\eta_1+1)\Gamma(m+\eta_2+1)}{(2m+\eta_1+\eta_2+1)\Gamma(m+\eta_1+\eta_2+1)m!}. \tag{53}$$

Note that $p_0^{(s,t)}(x) = 1$. Therefore, one can easily show by using the orthogonality property (52) that the proposed solution (50) automatically satisfies the compatibility condition (47).

Substituting (50) into (46) and making use of (B2) yields

$$\frac{\sqrt{1-\beta^2}}{2} \sum_{n=1}^{N} \mathbf{D}\mathbf{Q}_{n-1}(x)\mathbf{c}_n + k_0 \sum_{n=1}^{N} \left\{ \int_{-1}^{1} \mathbf{H}(\xi - x)\mathbf{W}(\xi)\mathbf{P}_n(\xi)\,\mathrm{d}\xi \right\} \mathbf{c}_n = \mathbf{q}(x), \quad |x| < 1, \tag{54}$$

where $\mathbf{Q}_{m-1}(x)$ is given by (B4). Next, pre-multiply (54) by $\mathbf{Q}_{m-1}(x)\mathbf{W}^{-1}(x)$ and integrate it from -1 to 1 with respect to x. This gives a system of equations for $\mathbf{c}_n$

$$\sum_{n=1}^{N} (\mathbf{V}_{mn} + y_m\delta_{mn}\mathbf{D})\mathbf{c}_n = \mathbf{s}_m, \quad m = 1, 2, 3, \ldots, N, \tag{55}$$

where

$$y_m = \sqrt{1-\beta^2}\,\Gamma(m-\eta_1)\Gamma(m-\eta_2)/[m!]^2, \tag{56}$$

$$\mathbf{V}_{mn} = k_0 \int_{-1}^{1} \int_{-1}^{1} \mathbf{Q}_{m-1}(x)\mathbf{W}^{-1}(x)\mathbf{H}(\xi - x)\mathbf{W}(\xi)\mathbf{P}_n(\xi)\,\mathrm{d}\xi\,\mathrm{d}x, \tag{57}$$

$$\mathbf{s}_m = \int_{-1}^{1} \mathbf{Q}_{m-1}(x)\mathbf{W}^{-1}(x)\mathbf{q}(x)\,\mathrm{d}x. \tag{58}$$

In deriving (55), the orthogonality property (52) has been used. By using (B6)–(B7), (57) and (58) can be further simplified to

$$\mathbf{V}_{mn} = v_{mn} \int_{-\infty}^{\infty} \mathrm{i}(k_0)^{m+n}(\mathrm{i}\xi)^{m+n-2}\mathbf{G}_m(\xi k_0)\mathbf{M}_0(\xi)\mathbf{F}_n(\xi k_0)\,\mathrm{d}\xi, \tag{59}$$

$$\mathbf{s}_m = \frac{2^{m+1}(\mathrm{i}ak_\alpha^{(1)}\sin\theta_i)^{m-1}}{(m-1)!} \exp(-\mathrm{i}ak_\alpha^{(1)}\sin\theta_i)B(m-\eta_1, m-\eta_2)\mathbf{G}_m(-ak_\alpha^{(1)}\sin\theta_i)\mathbf{q}_\alpha, \tag{60}$$

where

$$v_{mn} = \frac{(-1)^{m-1}2^{m+n+1}}{(m-1)!n!} B(m-\eta_1, m-\eta_2)B(n+1+\eta_1, n+1+\eta_2), \tag{61}$$

$$\mathbf{M}_0(\xi) = \frac{\mathrm{i}}{2\pi}\mathbf{R}^{-1}\mathbf{I}_0^{-1}[\mathrm{i}\xi\beta\mathbf{I}_0 - |\xi|\mathbf{I} - \mathbf{M}(\xi)/m]\mathbf{R}, \tag{62}$$

$$\mathbf{G}_m(x) = \begin{bmatrix} {}_1F_1(m-\eta_2; 2m-\eta_1-\eta_2; -2\mathrm{i}x) & 0 \\ 0 & {}_1F_1(m-\eta_1; 2m-\eta_1-\eta_2; -2\mathrm{i}x) \end{bmatrix}, \tag{63}$$

$$\mathbf{F}_m(x) = \begin{bmatrix} {}_1F_1(n+1+\eta_2; 2n+2+\eta_1+\eta_2; 2\mathrm{i}x) & 0 \\ 0 & {}_1F_1(n+1+\eta_1; 2n+2+\eta_1+\eta_2; 2\mathrm{i}x) \end{bmatrix}, \tag{64}$$

and $\mathbf{q}_\alpha$ is a vector dependent on the type of incident waves and the angle of incidence [see (A10)]. In (60)–(64), $B(x, y)$ is the Beta function, and ${}_1F_1(x; y; z)$ is the confluent hypergeometric function (Abramowitz and Stegun, 1972).

Equation (55) gives N algebraic equations for $\mathbf{c}_1, \mathbf{c}_2, \ldots, \mathbf{c}_n$. Once these equations are solved, an approximate solution to $\mathbf{g}(x)$ is obtained from (50). Clearly, the major numerical computation in this procedure is the evaluation of $\mathbf{V}_{mn}$ given by (59). In addition to the branch points introduced by (16), the integrand may also have poles on the real ξ-axis corresponding to the Stoneley wave (Achenbach, 1973). Although the Stoneley poles occur only for a very restrictive class of solids (Scholte, 1947), care must be taken when they are present. For example, the technique of deforming the contour of integration below the real ξ-axis may be used (Keer *et al.*, 1984).

To evaluate $\mathbf{V}_{mn}$ numerically, the infinite integral needs to be truncated. This does not seem to be a problem because the integrand tends to zero at infinity very fast, especially for large m or n. In the numerical example given below, the integration limits were taken from -5 to 5, which gives errors of less than a few percent even for k_0 as high as 10.

The other parameter concerning the accuracy of the numerical solution is the number of terms in the expansion, N. It is apparent from the properties of the confluent hypergeometric function that the value of $\mathbf{V}_{mn}$ decreases extremely fast as m or n increases. For instance, for $k_0 = 5$, in the numerical example given in Section 7,

$$\mathbf{V}_{11} = \begin{bmatrix} 3.5-0.7\mathrm{i} & -0.1-1.4\mathrm{i} \\ -0.1-1.4\mathrm{i} & -3.5+0.7\mathrm{i} \end{bmatrix}, \quad \mathbf{V}_{55} = \begin{bmatrix} 0.05-0.06\mathrm{i} & -0.03-0.004\mathrm{i} \\ -0.03-0.004 & -0.05+0.06\mathrm{i} \end{bmatrix}.$$

It is therefore concluded that $N = 5$ will yield adequate accuracy for moderate frequencies ($k_0 \approx 5$).

To close this section, it should also be mentioned that an advantage of the numerical approach presented here is that many integrals are carried out analytically in terms of special functions. Since these special functions are well tabulated and implemented in many FORTRAN packages (such as IMSL), programming of this solution procedure becomes very simple.

5. CRACK-TIP FRACTURE PARAMETERS

In this section, two important fracture mechanics parameters, namely, stress intensity factors and crack opening displacement, are derived in terms of the dislocation density solved from Section 4.

First, consider the stress intensity factors. It follows from (37) that the traction on the interface outside the crack is given by

$$\mathbf{t}(ax,0)=\begin{bmatrix}\sigma_{12}\\ \sigma_{22}\end{bmatrix}=-\frac{m}{\pi}\int_{-1}^{1}\frac{\mathbf{f}(a\eta)}{\eta-x}\,\mathrm{d}\eta+mk_0\int_{-1}^{1}\mathbf{K}(a\eta-ax)\mathbf{f}(a\eta)\,\mathrm{d}\eta. \tag{65}$$

The stress intensity vector, e.g. at $x_1=a$ $(x=1)$, may be defined by

$$\mathbf{k}=\begin{bmatrix}K_{II}\\ K_I\end{bmatrix}=\lim_{x\to 1^+}\{\sqrt{2\pi a(x-1)}\,\mathbf{R}\hat{\mathbf{W}}^{-1}(x)\mathbf{R}^{-1}\mathbf{t}(ax,0)\}, \tag{66}$$

where $\hat{\mathbf{W}}(x)$ is defined in (B5).

Note that the second term on the right-hand side of (65) is bounded at $x=1$. Therefore, making use of (45a) and (50) in (66) yields

$$\mathbf{k}=\lim_{x\to 1^+}\left\{m\sqrt{2\pi a(x-1)}\,\mathbf{R}\hat{\mathbf{W}}^{-1}(x)\sum_{n=1}^{N}\left[\frac{1}{\pi}\int_{-1}^{1}\mathbf{W}(s)\mathbf{P}_n(s)\frac{\mathrm{d}s}{s-x}\right]\mathbf{c}_n\right\}. \tag{67}$$

It then follows from (B3) that

$$\begin{aligned}\mathbf{k}&=\lim_{x\to 1^+}\left\{m\sqrt{\pi a}\,\mathbf{R}\hat{\mathbf{W}}^{-1}(x)\sum_{n=1}^{N}[-\sqrt{1-\beta^2}\,\hat{\mathbf{W}}(x)\mathbf{P}_n(x)]\mathbf{c}_n\right\}\\&=-m\sqrt{\pi a(1-\beta^2)}\,\mathbf{R}\sum_{n=1}^{N}\mathbf{P}_n(1)\mathbf{c}_n.\end{aligned} \tag{68}$$

Consequently, the crack-tip singular field at $x_1=a$ $(x=1)$ can be written as

$$\mathbf{t}(ax,0)=\frac{1}{\sqrt{2\pi a(x-1)}}\mathbf{R}\hat{\mathbf{W}}(x)\mathbf{R}^{-1}\mathbf{k}. \tag{69}$$

It is seen that the crack-tip singular fields are oscillatory as in the corresponding static case. It is also seen from (66) and (69) that, K_I (K_{II}) does not represent the opening (shearing) fracture mode as it does in the homogeneous case. The two fracture modes are always coupled. Consequently, K_{II} is not zero even for normal incidence of longitudinal waves.

Next, consider the crack opening displacement. It follows from (22) and (50) that

$$\Delta\mathbf{u}(ax)=a\mathbf{R}\sum_{n=1}^{N}\left[\int_{-1}^{x}\mathbf{W}(s)\mathbf{P}_n(s)\,\mathrm{d}s\right]\mathbf{c}_n. \tag{70}$$

By using the Rodrigues formula (Abramowitz and Stegun, 1972), an alternative expression of the crack opening displacement may be given as

$$\Delta\mathbf{u}(ax)=a\mathbf{R}\sum_{n=1}^{N}\left\{\frac{(-1)^n}{2^n n!}\frac{\mathrm{d}^{n-1}}{\mathrm{d}x^{n-1}}[(1-x^2)^n\mathbf{W}(x)]\right\}\mathbf{c}_n. \tag{71}$$

The near tip behavior can be examined by letting $x\to\pm 1$. For example, at the right crack tip $(x_1=a)$, the crack opening displacement can be written asymptotically as

$$\Delta\mathbf{u}(ax)\approx-\frac{a}{\sqrt{2}}\sqrt{1-x}\,\mathbf{R}\hat{\mathbf{W}}(x)\sum_{n=1}^{N}\mathbf{P}_n(1)\mathbf{c}_n,\quad \text{as } x\to 1. \tag{72}$$

Because of the oscillatory behaviour, the normal crack opening displacement changes its sign an infinite number of times as x approaches the crack tip $(x\to 1)$. This indicates material interpenetration, which violates the compatibility of deformation. In addition, the crack face interpenetration will create non-zero traction on the crack face, which contradicts

the crack face traction-free assumption specified by (8c). This pathological behavior was found for interface cracks under static loading [e.g. see England (1965)]. Equation (72) indicates that interface cracks under dynamic loading behave the same way. Similar to the static case, the size of the area over which the crack faces come into contact is independent of the magnitude of loads. However, it does depend on the incident frequency.

Another quantity of practical interest is the crack opening area:

$$\mathbf{v} = \int_{-a}^{a} \Delta\mathbf{u}(x_1)\,dx_1 = a^2\mathbf{R}\sum_{n=1}^{N}\left[\int_{-1}^{1}\int_{-1}^{x}\mathbf{W}(s)\mathbf{P}_n(s)\,ds\,dx\right]\mathbf{c}_n. \tag{73}$$

By interchanging the order of integration, (73) can be rewritten as

$$\mathbf{v} = -a^2\mathbf{R}\sum_{n=1}^{N}\left[\int_{-1}^{1}\mathbf{W}(s)\mathbf{P}_n(s)s\,ds\right]\mathbf{c}_n. \tag{74}$$

Note that $\mathbf{P}_0(x) = \mathbf{I}$. Therefore, it follows from the orthogonality condition (52) and the Rodrigues formula (Abramowitz and Stegun, 1972) that

$$\mathbf{v} = a^2\Gamma(2+\eta_1)\Gamma(2+\eta_2)\mathbf{R}\mathbf{c}_1. \tag{75}$$

It is interesting to note that $\mathbf{v}$ depends on $\mathbf{c}_1$ only.

6. NON-OSCILLATORY SINGULAR FIELDS

It is seen from the previous section that the crack-tip singular stress fields are oscillatory and crack faces come into contact near the crack tips. This pathological behavior of the solution contradicts the boundary conditions set forth for the boundary value problem. Theoretically speaking, therefore, the solution obtained in Section 5 is not valid. For this reason, Comninou (1977) proposed a contact zone model for interface cracks under static loading. In her model, oscillation and interpenetration are eliminated by allowing the crack faces to come into contact in the boundary conditions of the boundary value problem. Studies of dynamically loaded cracks using Comninou's contact zone model are undertaken. The results will be reported elsewhere. In this section, an opportunistic approach is taken to remedy the pathological behavior possessed by the solutions obtained in Section 5.

It is apparent that the source of the pathological crack tip fields is the matrix $\hat{\mathbf{W}}(x)$. Notice that when $\varepsilon = 0$, $\hat{\mathbf{W}}(x)$ will become an identity matrix, and consequently, the pathological behavior will disappear. It has been shown by Dundurs (1969) that the bimaterial constant β is limited by $0 \leqslant |\beta| < 0.5$. Furthermore, data by Suga *et al.* (1988) on over 100 material pairs suggest that the values of β are even more restricted, i.e. $|\beta| < 0.25$, implying that $|\varepsilon| < 0.08$. For instance, the numerical example given in Section 7 has $\beta = 0.06831$, which corresponds to $\varepsilon = 0.02178$. Since $\lim_{\varepsilon\to 0}\hat{\mathbf{W}}(x) = \mathbf{I}$, we may therefore treat $\hat{\mathbf{W}}(x) = \mathbf{I}$ for all practical purposes. By adopting this engineering approximation, the crack-tip singular stress fields at $x_1 = a$ ($x = 1$) can be written as

$$\tau(x) = \frac{1}{\sqrt{2\pi a(x-1)}}\mathbf{k}. \tag{76}$$

Obviously, the crack-tip singular fields are no longer oscillatory. Furthermore, K_{I} and K_{II} are now representatives of the crack-tip opening and shearing fracture modes, respectively. However, because of the mode mixity near the crack tip, even in this case K_{II} is still not zero for normal incidents of longitudinal waves, as will be seen from the numerical example given in the next section.

When $\hat{\mathbf{W}}(x) = \mathbf{I}$, the crack opening displacement of (71) and (72) will become, respectively,

$$\Delta\mathbf{u}(ax) = a\sum_{n=1}^{N}\left\{\frac{(-1)^n}{2^n n!}\frac{d^{n-1}}{dx^{n-1}}[(1-x^2)^{n-1/2}]\right\}\mathbf{R}\mathbf{c}_n, \quad |x| < 1 \tag{77}$$

and

$$\Delta\mathbf{u}(ax) \approx -\frac{a}{\sqrt{2}}\sqrt{1-x}\,\mathbf{R}\sum_{n=1}^{N}\mathbf{P}_n(1)\mathbf{c}_n, \quad \text{as } x \to 1. \tag{78}$$

Clearly, interpenetration of crack faces no longer occurs.

7. NUMERICAL RESULTS

In this section, a numerical example is given to illustrate the method of solution outlined in Section 5. In this example, the incident wave is taken to be a longitudinal plane wave from $x_2 = -\infty$. The material parameters used in the numerical computation are given in Table 1. For this material combination, our numerical search found that the integrand in (59) has no poles along the real ξ-axis. The coefficient $\mathbf{V}_{mn}$ is evaluated by integrating the integrand in (59) from -5 to 5. In the numerical solution, $N = 5$ is used in (50), i.e., there are 5 terms in the Jacobi polynomial expansion. These parameters are chosen on the basis that further increase of these values does not change the final solution by more than a few percent.

To present the numerical solutions in non-dimensional form, the corresponding static problems are solved first. Then, the dynamic solutions are normalized by the corresponding static solutions and are plotted in Figs 2–5.

For normal incidence, the mode I and mode II stress intensity factors versus non-dimensional wavenumber k_0 are plotted in Fig. 2(a). The stress intensity factors are normalized by the static, mode I stress intensity factor, i.e.

Table 1. Material properties for the Al/Cu interface. Al is material 1 and Cu is material 2

Materials	c_L	c_T	ν
Aluminum	$c_L^{(1)} = 6300$ m s^{-1}	$c_T^{(1)} = 3100$ m s^{-1}	$\nu_1 = 0.34$
Copper	$c_L^{(2)} = 4600$ m s^{-1}	$c_T^{(2)} = 2300$ m s^{-1}	$\nu_2 = 0.33$

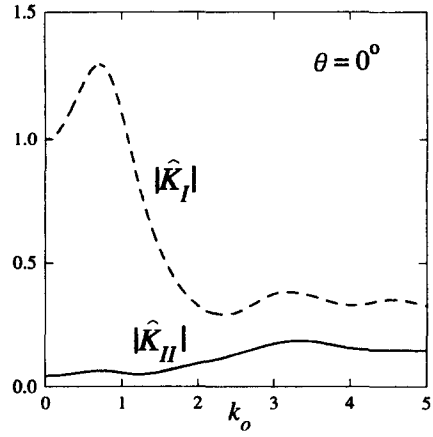

Fig. 2(a). Normalized stress intensity factor versus frequency for normal incidence.

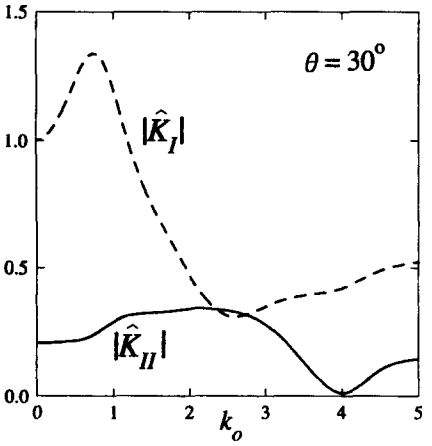

Fig. 2(b). Normalized stress intensity factor versus frequency for oblique incidence, $\theta = 30°$.

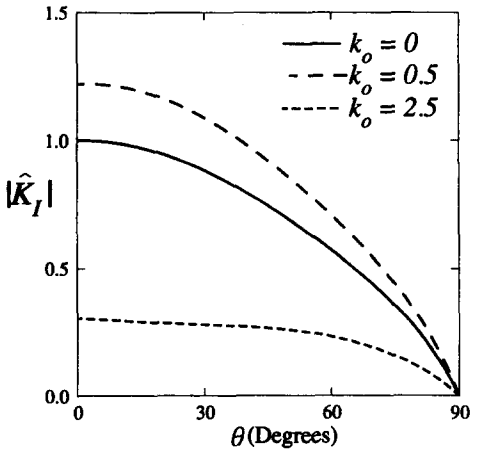

Fig. 3(a). Normalized mode I stress intensity factor versus incident angle for $k_0 = 0.0, 0.5, 2.5$.

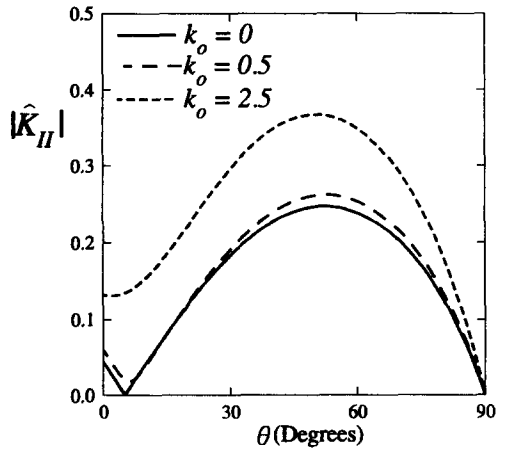

Fig. 3(b). Normalized mode II stress intensity factor versus incident angle for $k_0 = 0.0, 0.5, 2.5$.

$$\hat{\mathbf{k}} = \begin{bmatrix} \hat{K}_{II} \\ \hat{K}_I \end{bmatrix} = \frac{1}{K_I^{\text{static}}} \mathbf{k} = \frac{1}{K_I^{\text{static}}} \begin{bmatrix} K_{II} \\ K_I \end{bmatrix}. \tag{79}$$

It is observed that the mode II stress intensity factor is not zero although the incident

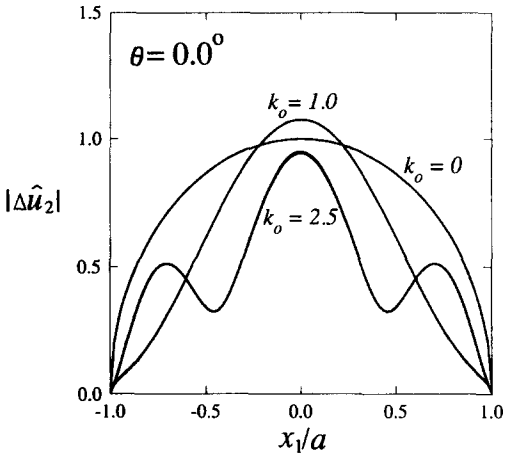

Fig. 4(a). Normalized crack opening displacement in the x_2-direction under normal incidence for $k_0 = 0.0, 1.0, 2.5$. Dotted lines (coincide with the solid lines) are from the oscillatory solution (71), while the solid lines are from the non-oscillatory solution (77).

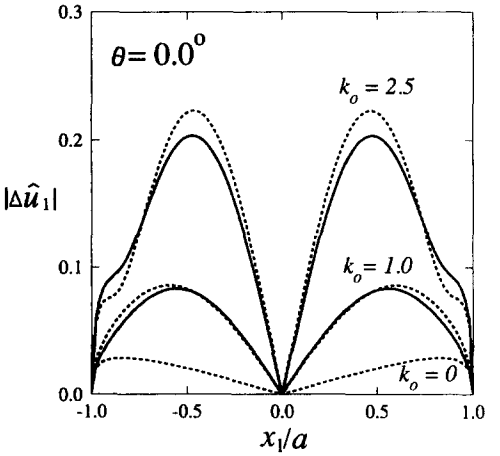

Fig. 4(b). Normalized crack opening displacement in the x_1-direction under normal incidence for $k_0 = 0.0, 1.0, 2.5$. Dotted lines are from the oscillatory solution (71), while the solid lines are from the non-iscillatory solution (77). The solid line corresponding to $k_0 = 0.0$ is $|\hat{\mathbf{u}}_2| = 0$.

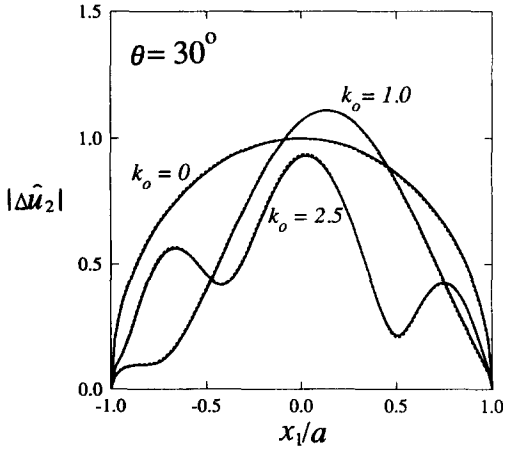

Fig. 5(a). Normalized crack opening displacement in the x_2-direction under oblique incidence, $\theta = 30°$, for $k_0 = 0.0, 1.0, 2.5$. Dotted lines are from the oscillatory solution (71), while the solid lines are from the non-oscillatory solution (77).

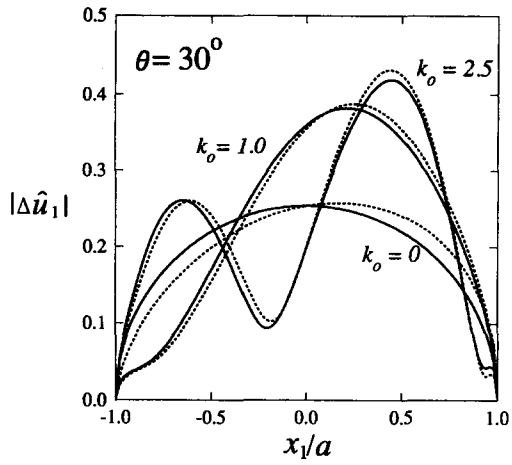

Fig. 5(b). Normalized crack opening displacement in the x_1-direction under oblique incidence, $\theta = 30°$, for $k_0 = 0.0, 1.0, 2.5$. Dotted lines are from the oscillatory solution (71), while the solid lines are from the non-oscillatory solution (77).

wave is normal to the interface. This mixed mode behavior is typical of interface cracks. It is also seen that the crack-tip field is dominated by the opening mode (mode I) at lower frequencies ($k_0 < 2$). However, at higher frequencies ($k_0 > 2$), mode I and mode II are in the same order of magnitude.

The normalized stress intensity factors for an oblique incidence, $\theta = 30°$, are presented in Fig. 2(b).

The stress intensity factors as functions of the incident angle, θ, are plotted in Figs 3(a) and 3(b) for $k_0 = 0.0, 0.5, 2.5$. The normalization factor K_I^{static} used in (79) is taken to be its value at normal incidence ($\theta_i = 0°$). As expected, Fig. 3(a) shows that $\hat{K}_I$ monotonically decreases to zero as the incident angle increases from normal incidence to grazing incidence. The mode II stress intensity factor, $\hat{K}_{II}$, seems to reach a maximum when the incident angle is about 50° as shown in Fig. 3(b).

The crack opening displacements are given in Figs 4–5 for $k_0 = 0.0, 1.0, 2.5$. They are normalized by the static value of normal opening at $x_1 = 0$, i.e.

$$\Delta\hat{\mathbf{u}} = \begin{bmatrix} \Delta\hat{u}_1 \\ \Delta\hat{u}_2 \end{bmatrix} = \frac{1}{\Delta u_2^{\text{static}}(0)} \Delta\mathbf{u} = \frac{1}{\Delta u_2^{\text{static}}(0)} \begin{bmatrix} \Delta u_1 \\ \Delta u_2 \end{bmatrix}. \tag{80}$$

On each plot, the dotted lines are from the oscillatory solution (71), while the solid lines are from the non-oscillatory solution (77).

Figure 4(a) shows the normal crack opening displacement for normal incidence. The dotted lines are not distinguishable from the solid lines, which indicates that taking $\hat{\mathbf{W}}(x) = \mathbf{I}$ produces very little difference in the opening mode. The shear crack opening displacement under normal incidence is presented in Fig. 4(b). Again, there exists very little difference between the oscillatory (dotted lines) and non-oscillatory (solid lines) solutions. The solid line corresponding to $k_0 = 0$ coincides with the x_1/a axis, since the shear opening is zero in the non-oscillatory case. It is interesting to note that the non-oscillatory solution yields zero shear opening displacement, but non-zero singular shear stresses under normal incidence.

For an oblique incidence, $\theta_i = 30°$, the corresponding crack opening displacements are presented in Figs 5(a, b).

Acknowledgements—This work is partially supported by NSF under Grant MSS-9110291.

REFERENCES

Abramowitz, M. and Stegun, I. A. (1972). *Handbook of Mathematical Functions*. Dover, New York.
Achenbach, J. D. (1973). *Wave Propagation in Elastic Solids*. North Holland, Oxford.
Achenbach, J. D. and Gautesen, A. K. (1978). A ray theory for elastodynamic stress-intensity factors. *J. Appl. Mech.* **45**, 123–129.

Boström, A. (1987). Elastic wave scattering from an interface crack: Antiplane strain. *J. Appl. Mech.* **54,** 503–508.
Comninou, M. (1977). The interface crack. *J. Appl. Mech.* **44,** 631–636.
Dundurs, J. (1969). Discussion. *J. Appl. Mech.* **36,** 650–652.
England, A. H. (1965). A crack between dissimilar media. *J. Appl. Mech.* **32,** 400–402.
Erdogan, F. (1965). Stress distribution in bonded dissimilar materials with cracks. *J. Appl. Mech.* **32,** 403–410.
Erdogan, F. (1969). Approximate solutions of systems of singular integral equations. *SIAM J. Appl. Math.* **17,** 1041–1059.
Karpenko, L. N. (1966). Approximate solutions of a singular integral equation by means of Jacobi polynomials. *J. Appl. Math. Mech.* **30,** 668–675.
Keer, L. M., Lin, W. and Achenbach, J. D. (1984). Resonance effects for a crack near a free surface. *J. Appl. Mech.* **51,** 65–70.
Lighthill, M. J. (1964) *Introduction to Fourier Analysis and Generalized Functions.* Cambridge University Press.
Mal, A. K. (1970a). Interaction of elastic waves with a Griffith crack. *Int. J. Engng Sci.* **8,** 763–776.
Mal, A. K. (1970b). Interaction of elastic waves with a penny-shaped crack. *Int. J. Engng Sci.* **8,** 381–338.
Muskhelishvili, N. I. (1953). *Singular Integral Equations.* Noordhoff, Groningen, Holland.
Qu, J. and Bassani, J. L. (1989). Cracks on bimaterial and bicrystal interfaces. *J. Mech. Phys. Solids* **37,** 417–433.
Qu, J. and Li, Q. (1991). Interfacial dislocation and its application to interface cracks in anisotropic bimaterials. *J. Elasticity* **26,** 169–195.
Rice, J. R. and Sih, G. C. (1965). Plane problem of cracks in dissimilar media. *J. Appl. Mech.* **32,** 418–423.
Scholte, J. G. (1947). The range of existence of Rayleigh and Stoneley waves. *Monthly Notices R. Astron. Soc.* **5,** 120–126.
Suga, T. Elssner, E. and Schmander, S. (1988). Composite parameters and mechanical compatibility of material joints. *J. Compos. Mater.* **22,** 917–934.
Suo Z. (1991). Singularities interfaces and cracks in dissimilar antisotropic media. *Proc. R. Soc. Lond.* **A427,** 331–358.
Williams, M. L. (1959). The stress around a fault or crack in dissimilar media. *Bull. Seis. Soc. Amer.* **49,** 199–204.
Willis, J. R. (1971). Fracture mechanics of interface cracks. *J. Mech. Phys. Solids* **19,** 353–368.
Yang, H. J. and Bogy, D. B. (1985). Elastic wave scattering from an interface crack in a layered half-space. *J. Appl. Mech.* **52,** 42–50.

APPENDIX A

According to (11), $\mathbf{t}_0$ is the traction on the interface in the absence of the crack. It can be calculated if the coefficient of reflection from a solid–solid interface is known. However, the expression of the coefficient of reflection is rather complicated [e.g. see Achenbach (1973)]. In this section, an alternative method is developed to obtain $\mathbf{t}_0$ directly, without calculating the reflection coefficients.

First, consider the incident wave given by eqn (1). The traction on the interface corresponding to eqn (1) is

$$\mathbf{t}^{(i)}(x_1,0) = \mathrm{i}u_0\mu_1 k_\alpha^{(1)}\mathbf{v}^{(\alpha)}\exp(\mathrm{i}ak_\alpha^{(1)}x_1 p_1), \tag{A1}$$

where

$$\mathbf{v}^{(\alpha)} = \begin{bmatrix} p_1 d_2^{(\alpha)} + p_2 d_1^{(\alpha)} \\ (c_L^{(1)}/c_T^{(1)})^2 p_2 d_2^{(\alpha)} + [(c_L^{(1)}/c_T^{(1)})^2 - 2] p_1 d_1^{(\alpha)} \end{bmatrix}. \tag{A2}$$

To solve for the reflection and transmission problem, let the reflected and transmitted fields be represented by (13) and (18). Then, continuity of total displacement and traction on the interface gives

$$\int_{-\infty}^{\infty} (\mathbf{A}_2\mathbf{b}_2 - \mathbf{A}_1\mathbf{b}_1)\exp(-\mathrm{i}\xi x_1 k_T^{(1)})\,\mathrm{d}\xi = u_0\mathbf{d}^{(\alpha)}\exp(\mathrm{i}k_\alpha^{(1)}x_1 p_1), \tag{A3}$$

$$\int_{-\infty}^{\infty} (\mathbf{B}_2\mathbf{b}_2 - \mathbf{B}_1\mathbf{b}_1)\exp(-\mathrm{i}\xi x_1 k_T^{(1)})\,d\xi = \mathrm{i}\mu_1 u_0 k_\alpha^{(1)}\mathbf{v}^{(\alpha)}\exp(\mathrm{i}k_\alpha^{(1)}x_1 p_1). \tag{A4}$$

Application of the Fourier transform to (A3)–(A4) in conjunction with (34a) yields a system of equations for $\mathbf{b}_1$ and $\mathbf{b}_2$:

$$\mathbf{A}_2\mathbf{b}_2 - \mathbf{A}_1\mathbf{b}_1 = u_0\mathbf{d}^{(\alpha)}\delta(\xi + p_1 k_\alpha^{(1)}), \tag{A5}$$

$$\mathbf{B}_2\mathbf{b}_2 - \mathbf{B}_1\mathbf{b}_1 = \mathrm{i}\mu_1 u_0 k_\alpha^{(1)}\mathbf{v}^{(\alpha)}\delta(\xi + p_1 k_\alpha^{(1)}). \tag{A6}$$

Solving (A5)–(A6) yields

$$\mathbf{B}_2\mathbf{b}_2 = u_0\mathbf{M}(\mathbf{d}^{(\alpha)} - \mathrm{i}\mu_1 k_\alpha^{(1)}\mathbf{A}_1\mathbf{B}_1^{-1}\mathbf{v}^{(\alpha)})\delta(\xi + p_1 k_\alpha^{(1)}), \tag{A7}$$

where $\mathbf{M}$ is defined by (25). Substitution of (A7) into (18) for $n = 2$ gives the total traction on the interface

$$\mathbf{t}_0(ax,0) = \mathbf{t}_\alpha \exp[iak_\alpha^{(1)} x p_1], \tag{A8}$$

where

$$\mathbf{t}_\alpha = u_0 k_T^{(1)} \mathbf{M}(-p_1 k_\alpha^{(1)})[\mathbf{d}^{(\alpha)} - i\mu_1 k_\alpha^{(1)} \mathbf{A}_1(-p_1 k_\alpha^{(1)}) \mathbf{B}_1^{-1}(-p_1 k_\alpha^{(1)}) \mathbf{v}^{(\alpha)}], \quad \alpha = L, T. \tag{A9}$$

Then, according to (45c):

$$\mathbf{q}_\alpha = \mathbf{R}^{-1} \mathbf{I}_0^{-1} \mathbf{t}_\alpha / m.$$

In fact, the coefficients of reflection and transmission can also be obtained by substituting $\mathbf{b}_1$ and $\mathbf{b}_2$ into (13). The solutions so obtained are in matrix form and are easier to implement in the computer.

APPENDIX B

Define an analytical function $w(\eta_1, \eta_2, z) = (1-z)^{\eta_1}(1+z)^{\eta_2}$ in the complex plane $z = x+iy$, where η_1 and η_2 are given by (49a). The branch cut is taken along the real axis from $z = -1$ to $z = 1$, so that $w(\eta_1, \eta_2, x+i0) \equiv w_+(\eta_1, \eta_2, x) = (1-x)^{\eta_1}(1+x)^{\eta_2}$ for $|x| < 1$. Then, the following identity was derived by Karpenko (1966):

$$\frac{1}{\pi}\int_{-1}^{1} \frac{P_n^{(\eta_1,\eta_2)}(\zeta) w(\eta_1,\eta_2,\zeta)}{\zeta - z}\, d\zeta = \frac{1}{\sin \pi\eta_1}[e^{i\pi\eta_1} P_n^{(\eta_1,\eta_2)}(z) w(\eta_1,\eta_2,z) - 2^{-1} P_{n-1}^{(-\eta_1,-\eta_2)}(z)]. \tag{B1}$$

From (B1), it follows that for $n \geqslant 1$:

$$\frac{1}{\pi}\int_{-1}^{1} \mathbf{W}(s)\mathbf{P}_n(s)\frac{ds}{s-x} = \beta \mathbf{D}\mathbf{W}(x)\mathbf{P}_n(x) + \tfrac{1}{2}\sqrt{1-\beta^2}\,\mathbf{Q}_{n-1}(x), \quad |x| < 1, \tag{B2}$$

$$\frac{1}{\pi}\int_{-1}^{1} \mathbf{W}(s)\mathbf{P}_n(s)\frac{ds}{s-x} = \sqrt{1-\beta^2}\left\{\frac{-1}{\sqrt{x^2-1}}\hat{\mathbf{W}}(x)\mathbf{P}_n(x) + \tfrac{1}{2}\mathbf{Q}_{n-1}(x)\right\}, \quad x > 1, \tag{B3}$$

where

$$\mathbf{Q}_n(x) = \begin{bmatrix} P_n^{(-\eta_1,-\eta_2)} & 0 \\ 0 & P_n^{(-\eta_2,-\eta_1)}(x) \end{bmatrix}, \tag{B4}$$

$$\hat{\mathbf{W}}(x) = \begin{bmatrix} \left(\dfrac{x+1}{x-1}\right)^{i\varepsilon} & 0 \\ 0 & \left(\dfrac{x-1}{x+1}\right)^{i\varepsilon} \end{bmatrix}. \tag{B5}$$

To derive (59) from (57), the following identity must be used:

$$\int_{-1}^{1} (1-x)^{\eta_1}(1+x)^{\eta_2} P_n^{(\eta_1,\eta_2)}(x) \exp(iyx)\, dx$$

$$= \frac{2^{n+1+\eta_1+\eta_2}}{n!} \exp(-iy) B(n+1+\eta_1, n+1+\eta_2)\, {}_1F_1(n+1+\eta_2, 2n+2+\eta_1+\eta_2, 2iy),$$

which can be proved by using the Rodrigues formula (Abramowitz and Stegun, 1972) and integration by parts. Making use of this identity, one can show that

$$\int_{-1}^{1} \mathbf{W}(x)\mathbf{P}_n(x)\exp(iyx)\, dx = \frac{2^{n+1+\eta_1+\eta_2}(iy)^n}{n!} \exp(-iy) B(n+1+\eta_1, n+1+\eta_2)\mathbf{F}_n(y), \tag{B6}$$

$$\int_{-1}^{1} \mathbf{Q}_{m-1}(x)\mathbf{W}^{-1}(x)\exp(-iyx)\, dx = \frac{2^{m-\eta_1-\eta_2}(-iy)^m}{(m-1)!} \exp(iy) B(m-\eta_1, m-\eta_2)\mathbf{G}_m(y), \tag{B7}$$

where $\mathbf{F}_n(y)$ and $\mathbf{G}_m(y)$ are defined by (63) and (64), respectively.